Achieving High Order Fluctuation Splitting Schemes by Extending the Stencil.

M.E.Hubbard∗ and A.L.Laird†,
∗ *University of Leeds, Computational PDEs Unit, School of Computing, Leeds, LS2 9JT, U.K.* ,
† *University of Oxford, Oxford University Computing Laboratory, Wolfson Building, Parks Road, Oxford, OX1 3QD, U.K.* ,
E-mail: meh@comp.leeds.ac.uk, Alistair.Laird@comlab.ox.ac.uk

Version: 10th September 2003

An extension to the fluctuation splitting approach for approximating hyperbolic conservation laws is described, which achieves higher than second order accuracy in both space and time by extending the range of the distribution of the fluctuations. Initial results are presented for a simple linear scheme which is third order accurate in both space and time on uniform triangular grids. Numerically induced oscillations are suppressed by applying the flux-corrected transport algorithm. These schemes are evaluated in the context of existing fluctuation splitting approaches to modelling time-dependent flows and some suggestions for their future development are made.

Key Words: Time-Dependent, High Order Accuracy, Fluctuation Splitting, Positivity, Scalar Advection Equation.

1. INTRODUCTION

The fluctuation splitting approach to approximating multidimensional systems of conservation laws has now reached a stage where it can be used reliably to produce accurate approximations to steady state, fluid flow problems of a complexity relevant to industry [9], and are competitive with the best numerical methods available for modelling compressible fluid flow in more than one space dimension. The most successful of the schemes are based on the concept of upwinding and are able to reproduce most of the properties that have made upwind schemes so popular for solving one-dimensional problems: second order accuracy combined with positivity in the presence of discontinuities, and rapid convergence to the steady state, all without the necessity for additional artificial viscosity.

The success of the multidimensional fluctuation splitting schemes has been far more limited when they have been applied to time-dependent problems. The scalar PSI scheme [10] and its matrix distribution counterparts [16, 1], which are routinely used to compute high quality steady state solutions, drop to first order accuracy in space and time. They are surprisingly good at modelling flows with moving shocks, see for example [5], but their accuracy deteriorates dramatically in the presence of contact discontinuities. In fact, the basic scheme is incapable of modelling time-dependent linear advection adequately [12].

Initial attempts at addressing these problems [15, 11, 12] met with limited success, particularly when applied to nonlinear systems [17]. However, a variety of promising new approaches are starting to emerge: the space-time approaches of Csik and his coauthors [7, 8] and Abgrall and Mezine [2], the high order reconstruction of Caraeni *et al.* [6], and (potentially) the sub-cell distribution approach of Abgrall and Roe [3].

This paper presents an alternative approach, first implemented by Laird [13], to the problem of modelling time-dependent flows accurately, focusing initially on the approximation of the linear advection equation. The method retains the piecewise linear representation of the solution used by the steady state schemes, so the standard conservative linearisations are still valid and *any* of the methods normally used for decomposing nonlinear systems of equations can be simply combined with the scalar scheme. The improvement in accuracy is obtained by extending the range over which the fluctuation can be distributed. Third order accuracy in space can be achieved in a very compact manner, though higher orders would be considerably more complicated.

Comparable accuracy in time is achieved in two ways: (1) through the application of a TVD, Runge-Kutta discretisation [18] to the time derivative, and (2) use of a discrete form derived from the Lax-Wendroff approach, in which the Taylor series approximating the evolution of the system in time is rewritten in terms of spatial derivatives (via the original partial differential equation) which are then approximated to an appropriate order of accuracy. As they stand, the methods are not inherently positive, so unphysical oscillations are removed using Flux-Corrected Transport (FCT) [21, 14].

In Section 2, fluctuation splitting for the scalar advection equation (specifically,

the PSI scheme) will be described briefly. This is followed by a description of how the range of the distribution can be extended to give higher order spatial accuracy, along with the two methods of achieving the corresponding accuracy in time, the application of FCT, and a brief analysis of the stability of the resulting schemes. Section 4 contains a series of results obtained for the linear advection equation, illustrating the current capabilities of this approach, and the paper finishes with brief conclusions and suggestions for future work.

2. FLUCTUATION SPLITTING FOR ADVECTION

Consider the scalar conservation law,

$$u_t + f_x + g_y \;=\; 0 \qquad \text{or} \qquad u_t + \vec{\lambda} \cdot \vec{\nabla} u \;=\; 0 \tag{1}$$

where $\vec{\lambda} = \left(\frac{\partial f}{\partial u}, \frac{\partial g}{\partial u}\right)^{\mathrm{T}}$ defines the appropriate advection velocity. The fluctuation associated with this equation is a cell-based quantity which is given by

$$\phi \;=\; -\int\!\!\int_{\triangle} \vec{\lambda} \cdot \vec{\nabla} u \, \mathrm{d}x \, \mathrm{d}y \;=\; \oint_{\partial \triangle} u \, \vec{\lambda} \cdot \mathrm{d}\vec{n} \tag{2}$$

where $\vec{n}$ represents the inward pointing normal to the boundary of the cell.

The discrete form of ϕ is evaluated using an appropriate (conservative) linearisation [10]. When the integration in Eq. (2) can be carried out exactly the fluctuation can be written

$$\phi \;=\; -S_{\triangle} \widehat{\vec{\lambda}} \cdot \vec{\nabla} u \;=\; -\frac{1}{2} \sum_{i=1}^{3} u_i \, \widehat{\vec{\lambda}} \cdot \vec{n}_i \tag{3}$$

where $S_{\triangle}$ is the cell area and the symbol $\widehat{\cdot}$ indicates an appropriately linearised quantity. The index i loops over the vertices of the triangle and $\vec{n}_i$ is the inward unit normal to the i^{th} edge (opposite the i^{th} vertex) multiplied by the length of that edge. In the special case of linear advection a conservative linearisation can be constructed simply by assuming that u varies linearly over each triangle with the discrete solution values stored at the nodes and continuity across the edges of the grid cells [10].

A forward Euler discretisation of the time derivative leads to an iterative update of the nodal solution values which is generally written [10] as

$$u_i^{n+1} \;=\; u_i^n + \frac{\Delta t}{S_i} \sum_{j \in \cup \triangle_i} \alpha_i^j \phi_j \tag{4}$$

where S_i is the area of the median dual cell corresponding to node i (one third of the total area of the triangles with a vertex at i), α_i^j is the distribution coefficient which indicates the appropriate proportion of the fluctuation ϕ_j to be sent from cell j to node i, and $\cup\triangle_i$ represents the set of cells with vertices at node i. Conservation is assured as long as

$$\sum_{i\in\triangle_j} \alpha_i^j \;=\; 1 \qquad \forall j \tag{5}$$

where $\triangle_j$ represents the set of nodes at the vertices of cell j, *i.e.* the whole of each fluctuation is sent to the nodes. Note that the distribution has been restricted here so that a cell can only make contributions to nodes at its own vertices. This will be relaxed later on in order to obtain higher orders of accuracy.

2.1. The PSI Scheme

For steady state problems, the most commonly used scalar fluctuation splitting scheme is the PSI scheme, devised by Struijs [20] and formulated algebraically by Sidilkover and Roe [19] as follows.

1) For each triangle, locate the downstream vertices, *i.e.* those for which

$$\widehat{\vec{\lambda}}\cdot\vec{n}_i \;>\; 0 \tag{6}$$

where $\vec{n}_i$ is the inward pointing normal to the edge opposite vertex i.

2a) If a triangle has a single downstream vertex, node i say, then that node receives the whole fluctuation, so

$$u_i \;\rightarrow\; u_i + \frac{\Delta t}{S_i}\phi \tag{7}$$

while the values of u at the other two vertices remain unchanged.

2b) Otherwise, the triangle has two downstream vertices, i and j say, and the fluctuation is divided between these two nodes so that

$$u_i \;\rightarrow\; u_i + \frac{\Delta t}{S_i}\phi_i^* \qquad\qquad u_j \;\rightarrow\; u_j + \frac{\Delta t}{S_j}\phi_j^* \tag{8}$$

where $\phi_i^* + \phi_j^* = \phi$.

The fluctuations in Eq. (8) are defined as the limited quantities,

$$\phi_i^* \;=\; \phi_i - L(\phi_i, -\phi_j) \qquad\qquad \phi_j^* \;=\; \phi_j - L(\phi_j, -\phi_i) \tag{9}$$

where, following the N scheme [10],

$$\phi_i \;=\; -\frac{1}{2}\widehat{\vec{\lambda}}\cdot\vec{n}_i(u_i-u_k) \qquad\qquad \phi_j \;=\; -\frac{1}{2}\widehat{\vec{\lambda}}\cdot\vec{n}_j(u_j-u_k) \tag{10}$$

in which k denotes the remaining (upstream) vertex of the triangle and L denotes the minmod limiter function,

$$L(x,y) \;=\; \frac{1}{2}(1+\mathrm{sgn}(xy))\,\frac{1}{2}(\mathrm{sgn}(x)+\mathrm{sgn}(y))\min(|x|,|y|)\;. \tag{11}$$

The distribution coefficients, α_i^j in Eq. (4), can be derived easily from Eqs. (7)–(10), see [10]. The resulting scheme is globally positive and therefore conditionally stable, the appropriate restriction on the time-step being

$$\Delta t \;\le\; \frac{S_i}{\sum_{j\in\cup\triangle_i}\max\left(0,\frac{1}{2}\widehat{\vec{\lambda}_j}\cdot\vec{n}_i^j\right)} \tag{12}$$

This is the low order, non-oscillatory scheme which will be used later when the FCT algorithm is applied to the high order schemes described below. Note that it is only second order accurate *at the steady state*.

3. EXTENDING THE STENCIL

Existing fluctuation splitting schemes assume that the fluctuation within each grid cell will only be used to update the nodal solution values at the vertices of that cell. It is, however, simple to extend the range over which the fluctuation is distributed (and hence the stencil of the scheme) without seriously affecting the compactness of the scheme, although there would be a slight increase in inter-processor communication in any parallel implementation of the method.

In this work, the vertices of edge-neighbour cells are included in the distribution process, as illustrated in Figure 1. An additional memory (and parallel communication) overhead comes from the storage of 3 more nodes for each cell, and a little extra work is required in calculating the associated distribution coefficients, but the calculation of the fluctuations remains unchanged. Extending the stencil in such a way can achieve third order accuracy on grids with a regular connectivity. This leaves 3 degrees of freedom to be specified on a grid of equilateral triangles (2 too few to achieve fourth order accuracy) which can be used to give an adaptive stencil. Here, an upwind bias is introduced with stability and positivity in mind.

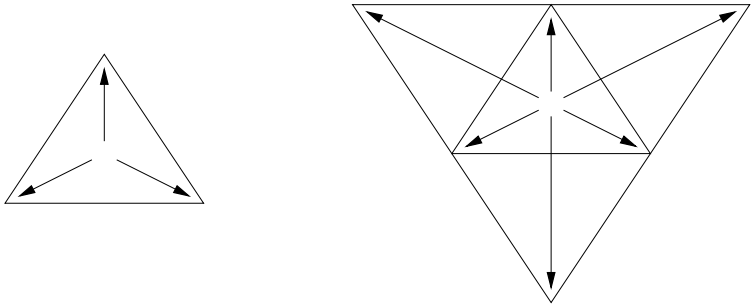

FIG. 1 The standard (left) and extended (right) distribution patterns for fluctuation splitting schemes.

The calculation of the fluctuation remains unchanged, as does the underlying representation of the solution, so these schemes can be extended simply to nonlinear systems of equations using *any* of the procedures previously suggested for steady state problems.

The nodal update at each time-step remains unchanged, *i.e.*

$$u_i^{n+1} \;=\; u_i^n + \frac{\Delta t}{S_i} \sum_{j \in \cup \triangle_i} \alpha_i^j \phi_j \tag{13}$$

except that, in addition to the cells with a vertex at node i, $\cup\triangle_i$ also contains all their edge-neighbour cells. In order to construct a third order discretisation, the distribution coefficients should be calculated so that

$$\frac{1}{S_i} \sum_{j \in \cup \triangle_i} \alpha_i^j \phi_j \;=\; (\vec{\lambda} \cdot \vec{\nabla} u)_i + \mathcal{O}(\delta^3) \tag{14}$$

in which δ is the local grid size.

The α_i^j are calculated here using Taylor series analysis on a regular triangular grid, constructed by bisecting each rectangle in a uniform Cartesian grid along the same diagonal (nominally top left to bottom right, though the analysis can be repeated for the opposite diagonal) - so the connectivity pattern is the same for every grid node. The algebra is extremely tedious so only the method is summarised, as follows.

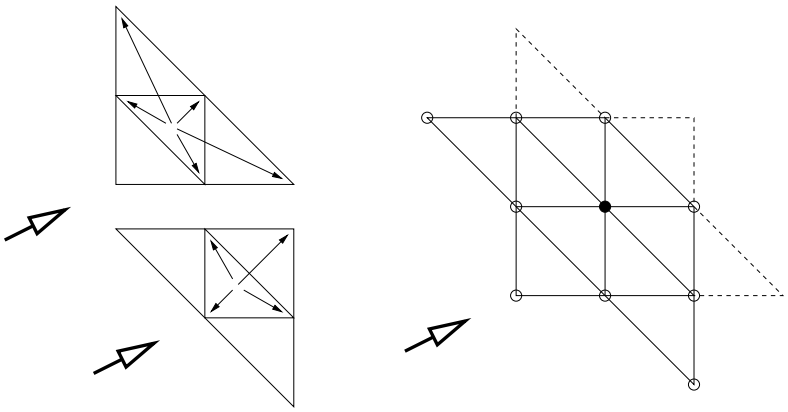

FIG. 2 Left: the upwind distribution of the cell fluctuation for triangles with two outflow edges (top) and with a single outflow edge (bottom). Right: the stencil (circled nodes) for updating the node denoted by the solid circle using the 'upwind' third order scheme. The large arrows indicate the advection velocity.

- Construct a set of coefficients A_k which satisfy

$$\sum_{\text{stencil}} A_k u_k \;=\; (\vec{\lambda}\cdot\vec{\nabla}u)_i + \mathcal{O}(\delta^3) \tag{15}$$

  giving a third order approximation to the nodal residual. The stencil in Eq. (15) is constructed in an upwind manner, *i.e.* contributions from a given cell are only sent to the vertices of that cell and vertices of edge-neighbour cells opposite outflow edges of the central cell, as illustrated in Figure 2. Note that this uniquely defines the A_k.

- Calculate the distribution coefficients α_i^j which satisfy

$$\frac{1}{S_i}\sum_{j\in\cup\triangle_i}\alpha_i^j\phi_j \;=\; \sum_{\text{stencil}} A_k u_k \tag{16}$$

  which ensures that Eq. (14) holds. This is manageable because each fluctuation ϕ is a linear combination of the solution values at the vertices of its cell.

The adaptive (upwind) stencil gives rise to two cases, precisely those of the PSI scheme, and these are illustrated in Figure 3. When a triangle has only one inflow

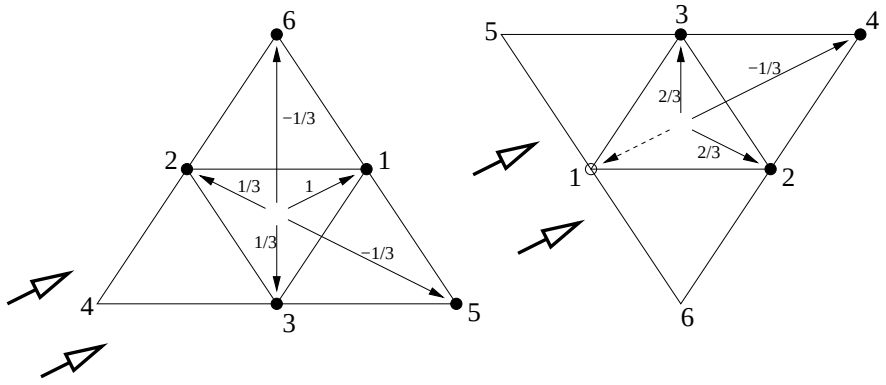

FIG. 3 The two cases for distribution: a cell with a single inflow edge (left) and a cell with two inflow edges (right). The distribution coefficients are shown in each case, and the large arrows indicate the advection velocity.

edge, the nodal updates due to its fluctuation ϕ can be expressed as

$$\begin{array}{lll} u_1 \rightarrow u_1 + \phi & u_2 \rightarrow u_2 + \frac{1}{3}\phi & u_3 \rightarrow u_3 + \frac{1}{3}\phi \\ u_4 \rightarrow u_4 & u_5 \rightarrow u_5 - \frac{1}{3}\phi & u_6 \rightarrow u_6 - \frac{1}{3}\phi \end{array} \tag{17}$$

The subscripts indicate the nodes, as numbered in the figure. Each node may also receive contributions from other triangles. For triangles with two inflow edges, the nodal contributions take the form

$$\begin{array}{lll} u_1 \rightarrow u_1 & u_2 \rightarrow u_2 + \frac{2}{3}\phi & u_3 \rightarrow u_3 + \frac{2}{3}\phi \\ u_4 \rightarrow u_4 - \frac{1}{3}\phi & u_5 \rightarrow u_5 & u_6 \rightarrow u_6 \end{array} \tag{18}$$

This scheme has been designed on a specific, uniform (and, in effect, structured) grid, but in this fluctuation distribution form it can be applied simply on any triangular grid, although it would be expected to lose accuracy as the grid changes shape and/or connectivity.

Initial numerical experiments verified the third order accuracy of the above scheme in space (it is only first order accurate in time) on uniform grids but, along with subsequent analysis, indicated that it is unconditionally unstable.

3.1. Improving Time-Accuracy, Stability and Positivity

The first approach to improving time-accuracy simply replaces the forward Euler discretisation of the time derivative by the third order, TVD Runge-Kutta scheme [18], given by

$$\begin{aligned} u^{(1)} &= u^n + \Delta t\, C[u^n] \\ u^{(2)} &= \frac{3}{4}u^n + \frac{1}{4}\left(u^{(1)} + \Delta t\, C[u^{(1)}]\right) \\ u^{n+1} &= \frac{1}{3}u^n + \frac{2}{3}\left(u^{(2)} + \Delta t\, C[u^{(2)}]\right) \end{aligned} \tag{19}$$

in which

$$C[u_i^n] \;=\; \frac{1}{S_i}\sum_{j\in\cup\triangle_i} \alpha_i^j \phi_j \tag{20}$$

The second method applies the Lax-Wendroff trick before discretisation, using the Taylor series expansion of $u(t+\Delta t)$ and the original differential equation, Eq. (1), to give

$$\begin{aligned} u_i^{n+1} &= u_i^n - \Delta t\left(\vec{\lambda}\cdot\vec{\nabla}u\right)_i^n + \frac{(\Delta t)^2}{2}\left[\vec{\lambda}\cdot\vec{\nabla}\left(\vec{\lambda}\cdot\vec{\nabla}u\right)\right]_i^n \\ &\quad -\frac{(\Delta t)^3}{6}\left(\vec{\lambda}\cdot\vec{\nabla}\left[\vec{\lambda}\cdot\vec{\nabla}\left(\vec{\lambda}\cdot\vec{\nabla}u\right)\right]\right)_i^n + \mathcal{O}((\Delta t)^4) \end{aligned} \tag{21}$$

This scheme is third order accurate in space and time if all of the space derivatives are approximated to the appropriate order, *i.e.* coefficients A_k, B_k and C_k are found such that

$$\begin{aligned} \left(\vec{\lambda}\cdot\vec{\nabla}u\right)_i^n &= \sum_{\text{stencil}} A_k u_k + \mathcal{O}(\delta^3) \\ \left[\vec{\lambda}\cdot\vec{\nabla}\left(\vec{\lambda}\cdot\vec{\nabla}u\right)\right]_i^n &= \sum_{\text{stencil}} B_k u_k + \mathcal{O}(\delta^2) \\ \left(\vec{\lambda}\cdot\vec{\nabla}\left[\vec{\lambda}\cdot\vec{\nabla}\left(\vec{\lambda}\cdot\vec{\nabla}u\right)\right]\right)_i^n &= \sum_{\text{stencil}} C_k u_k + \mathcal{O}(\delta) \end{aligned} \tag{22}$$

In fact, the Runge-Kutta approach serves a similar purpose, although it takes a different route to obtaining approximations of the appropriate order of accuracy.

The first derivative term in Eq. (22) can be discretised precisely as before, and the others can be approximated using a similar approach to that given by Eqs. (15) and (16) on the same uniform grid. Once again two cases arise in the distribution, depending on the number of inflow edges the central triangle has. For a single

inflow edge,

$$
\begin{aligned}
u_1 &\rightarrow u_1 + \left[1 + \frac{1}{2}\frac{\Delta t\, k_1}{S_\triangle} - \frac{1}{3}\left(\frac{\Delta t\, k_1}{S_\triangle}\right)^2\right]\phi \\
u_2 &\rightarrow u_2 + \left[\frac{1}{3} + \frac{1}{2}\frac{\Delta t\, k_2}{S_\triangle} + \frac{1}{6}\sum_{l=1}^{3}\left(\frac{\Delta t\, k_l}{S_\triangle}\right)^2 - \frac{2}{3}\left(\frac{\Delta t\, k_3}{S_\triangle}\right)^2\right]\phi \\
u_3 &\rightarrow u_3 + \left[\frac{1}{3} + \frac{1}{2}\frac{\Delta t\, k_3}{S_\triangle} + \frac{1}{6}\sum_{l=1}^{3}\left(\frac{\Delta t\, k_l}{S_\triangle}\right)^2 - \frac{2}{3}\left(\frac{\Delta t\, k_2}{S_\triangle}\right)^2\right]\phi \\
u_4 &\rightarrow u_4 \\
u_5 &\rightarrow u_5 + \left[-\frac{1}{3} + \frac{1}{3}\left(\frac{\Delta t\, k_2}{S_\triangle}\right)^2\right]\phi \\
u_6 &\rightarrow u_6 + \left[-\frac{1}{3} + \frac{1}{3}\left(\frac{\Delta t\, k_3}{S_\triangle}\right)^2\right]\phi
\end{aligned}
\tag{23}
$$

while for a triangle with two inflow edges,

$$
\begin{aligned}
u_1 &\rightarrow u_1 + \left[\frac{1}{2}\frac{\Delta t\, k_1}{S_\triangle} + \frac{1}{3}\left(\frac{\Delta t\, k_2}{S_\triangle}\right)^2 + \frac{1}{3}\left(\frac{\Delta t\, k_3}{S_\triangle}\right)^2\right]\phi \\
u_2 &\rightarrow u_2 + \left[\frac{2}{3} + \frac{1}{2}\frac{\Delta t\, k_2}{S_\triangle} - \frac{1}{6}\sum_{l=1}^{3}\left(\frac{\Delta t\, k_l}{S_\triangle}\right)^2\right]\phi \\
u_3 &\rightarrow u_3 + \left[\frac{2}{3} + \frac{1}{2}\frac{\Delta t\, k_3}{S_\triangle} - \frac{1}{6}\sum_{l=1}^{3}\left(\frac{\Delta t\, k_l}{S_\triangle}\right)^2\right]\phi \\
u_4 &\rightarrow u_4 + \left[-\frac{1}{3} + \frac{1}{3}\left(\frac{\Delta t\, k_1}{S_\triangle}\right)^2\right]\phi \\
u_5 &\rightarrow u_5 \\
u_6 &\rightarrow u_6
\end{aligned}
\tag{24}
$$

where $k_i = \frac{1}{2}\vec{\lambda}\cdot\vec{n}_i$ and $S_\triangle$ is the area of the triangle. The regions of linear stability for these schemes on a uniform grid were calculated numerically, in terms of the standard one-dimensional CFL numbers $\nu_x = \lambda_x \Delta t/\Delta x$ and $\nu_y = \lambda_y \Delta t/\Delta y$, and are shown in Figure 4. Note that swapping the orientation of the diagonals of the uniform triangular simply reflects the stability regions in one of the zero axes.

Both schemes are third order accurate in space and time, and conditionally stable, but neither is guaranteed to be positive, so unphysical oscillations can occur in the numerical solution. Here, this is dealt with using the Flux-Corrected Transport (FCT) algorithm which can combine either of the above schemes with the PSI scheme in a post-processing step which removes the unwanted oscillations. The FCT procedure for fluctuation distribution schemes is very close to that con-

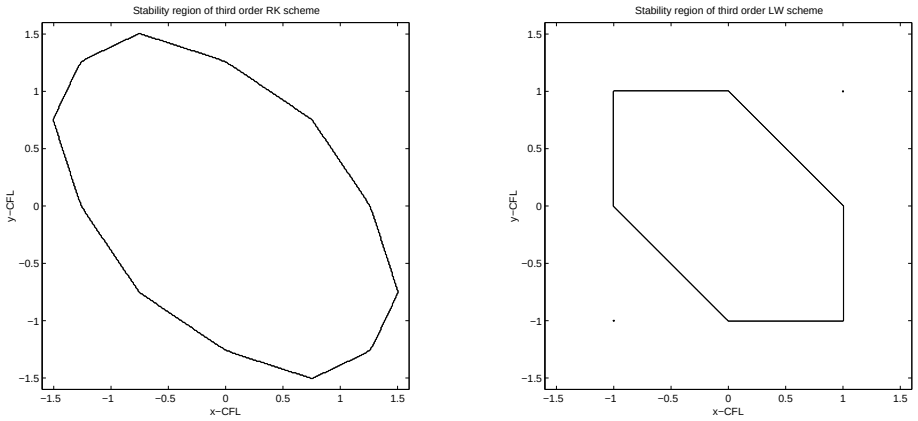

FIG. 4 The stability regions for the third order Runge-Kutta (left) and Lax-Wendroff (right) schemes. The grid used is constructed from a uniform rectangular grid divided into triangles by drawing diagonals from the top left to the bottom right vertices of each cell.

structed for finite element algorithms by Löhner *et al.* [14], and described in some detail in [12, 11]. It can be summarised by the following steps (i is used as a node index, j as a cell index):

1. For each cell: compute the low-order (LEC), high-order (HEC) and anti-diffusive (AEC = HEC − LEC) element contributions, noting that there are now 6 non-zero contributions in the high-order and anti-diffusive terms.

2. For each node: compute the updated low order approximation (as in Eq. (4)),

$$u_i^{\mathrm{L}} \;=\; u_i^n + \sum_{j \in \cup \triangle_i} \mathrm{LEC}_i^j \tag{25}$$

3. For each cell: correct the AEC to each of the 6 associated nodes so that conservation is retained and the new solution (as defined in step 4) has no extrema not also found in either u_i^{L} or u_i^n, so

$$\mathrm{AEC}_i^j \;\rightarrow\; \beta^j \times \mathrm{AEC}_i^j \;, \tag{26}$$

   where $0 \leq \beta^j \leq 1$. This involves

   (a) evaluating, in order, the quantities

$$u_i^* \quad = \quad \begin{Bmatrix} \max \\ \min \end{Bmatrix} (u_i^{\mathrm{L}}, u_i^n)$$

$$
\begin{aligned}
u_j^* &= \begin{cases}\max\\ \min\end{cases} u_i^* \qquad \forall\, i \in \triangle_j \\
u_i^{\substack{\max\\ \min}} &= \begin{cases}\max\\ \min\end{cases} u_j^* \qquad \forall\, j \in \cup\triangle_i
\end{aligned} \tag{27}
$$

the last of which give the extreme values of the solution at each node i, beyond which the updated solution is not allowed to go.

(b) defining

$$
\begin{aligned}
P_i^{\pm} &= \sum_{j\in\cup\triangle_i} \begin{matrix}\max\\ \min\end{matrix}(0, \mathrm{AEC}_i^j) \\
Q_i^{\pm} &= u_i^{\substack{\max\\ \min}} - u_i^{\mathrm{L}}
\end{aligned} \tag{28}
$$

and subsequently

$$
W_i^{\pm} = \begin{cases} \min\left(1, Q_i^{\pm}/P_i^{\pm}\right) & \text{if } P_i^+ > 0,\ P_i^- < 0 \\ 0 & \text{if } P_i^{\pm} = 0 \end{cases} \tag{29}
$$

a nodal limiting factor for the anti-diffusive contribution which ensures that the new solution value at node i does not violate the prescribed bounds.

(c) calculating

$$
\beta^j = \min_{i\in\triangle_j} \begin{cases} W_i^+ & \text{if } \mathrm{AEC}_i^j \geq 0 \\ W_i^- & \text{if } \mathrm{AEC}_i^j < 0 \end{cases} \tag{30}
$$

the limiting factor on the element→vertex contribution.

4. For each node: compute the final solution update,

$$
u_i^{n+1} = u_i^{\mathrm{L}} + \sum_{j\in\cup\triangle_i} \mathrm{AEC}_i^j \tag{31}
$$

The only difference between this and the standard approach is that the element contributions extend over a wider range (due to the larger stencil), which is accounted for when the limits on the nodal updates are calculated. In fact, FCT is not applied to the Runge-Kutta scheme in any of the results presented below because it would be very expensive to do so - either applying it at each stage or taking account of the hugely extended stencil of the overall scheme.

Note that, since the FCT algorithm simply requires a positive scheme to remove any spurious oscillations created by a high order method, it can be applied twice in this situation [13]. The first sweep can combine the PSI and Lax-Wendroff schemes

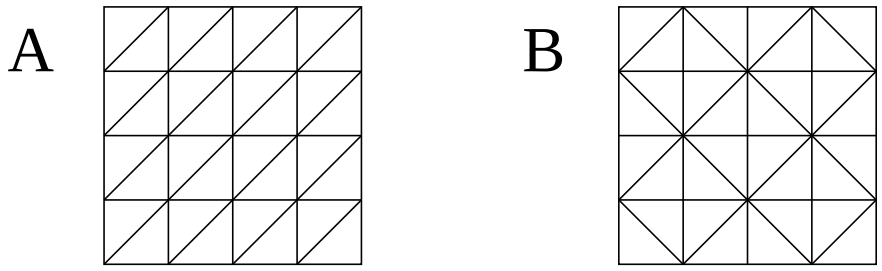

FIG. 5 The two types of grid used for the numerical experiments.

while the second sweep uses the resulting scheme (which is positive) with one of third order. The result is slightly more accurate than a direct combination of PSI and third order schemes [13], but the benefit is not enough to counteract the drop in speed of the algorithm, so it is not used here.

4. RESULTS

The first test case involves the advection of an initial double sine wave profile, given by

$$u \;=\; \sin(2\pi x)\sin(2\pi y) \tag{32}$$

with constant velocity $\vec{\lambda} = (1, 2)^{\mathrm{T}}$ over the domain $[0, 1] \times [0, 1]$. Periodic boundary conditions are applied throughout and the approximate and exact solutions are compared at $t = 1.0$ when they should both have returned to the initial profile. Unless stated otherwise, $\Delta t/\Delta x = 0.32$ for each computation, so that $|\nu_x| + |\nu_y| = 0.96$, well within the limits implied by the stability analysis for both schemes (see Figure 4).

The results of convergence studies carried out on a successively refined set of uniform grids (of the two types, A and B, shown in Figure 5) are illustrated in Figures 6 and 7. A comparison is made between the three third order methods (the Runge-Kutta scheme (RK3) and the Lax-Wendroff style scheme without (LW3) and with FCT (LW3+FCT)), two second order methods (the Lax-Wendroff scheme with FCT (LW2+FCT) and a standard cell-centred finite volume scheme on triangles - the MLG scheme of Batten *et al.* [4]) and the first order PSI scheme. Note that the results for the cell-centred scheme are shifted to the left in order to give a proper comparison in terms of the number of unknowns in the calculation.

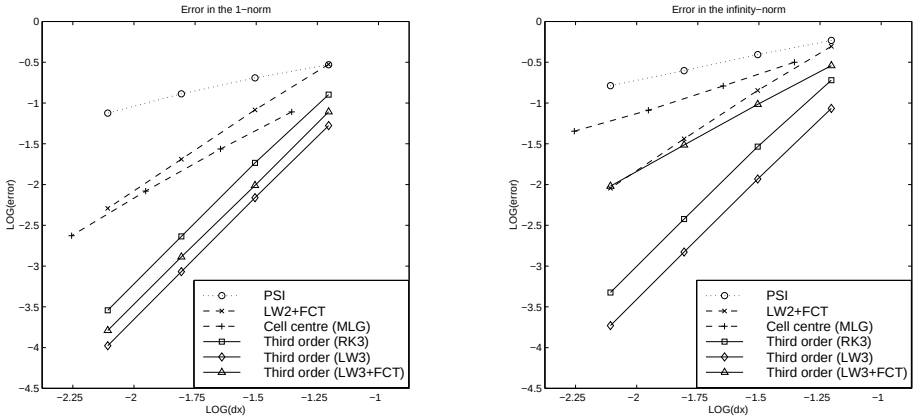

FIG. 6 Log-log graphs of error against grid size for the double sine wave test case on grid A. Third order schemes are represented by solid lines, second order by dashes and first order by dots.

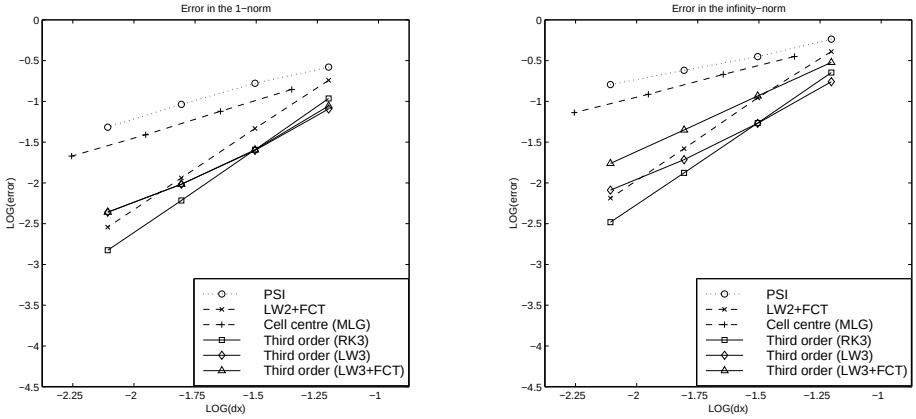

FIG. 7 Log-log graphs of error against grid size for the double sine wave test case on grid B. Third order schemes are represented by solid lines, second order by dashes and first order by dots.

	Double sine wave				Rotating cone	
	Grid A		Grid B		Grid A	Grid B
Scheme	l_1	l_∞	l_1	l_∞	Peak value	
PSI	0.79	0.61	0.93	0.58	0.33	0.35
LW2+FCT	2.00	2.01	2.01	2.02	0.76	0.76
Cell-centred (MLG)	1.82	0.85	0.87	0.75	0.87	0.49
Third Order (RK3)	3.01	2.99	2.03	2.01	0.81	0.86
Third Order (LW3)	3.02	3.00	1.14	1.24	0.83	0.86
Third Order (LW3+FCT)	3.00	1.67	1.14	1.36	0.76	0.77

TABLE 1

Numerical orders of accuracy for the constant advection of a doubly periodic sine wave, along with peak solution values on the 64×64 type A grid after a single period of the rotating cosine-squared profile.

In the L_1 norm, the new schemes show a clear improvement on grids of type A and, as predicted by the analysis, exhibit third order accuracy. The orders approximated on the finest grids are given in Table 1. In the L_∞ norm there is a notable loss of accuracy when FCT is applied, more than is the case for the Lax-Wendroff scheme, suggesting that the FCT algorithm is rather restrictive when an extended stencil is considered. As expected, given the change in connectivity, the order of accuracy drops significantly on type B grids, and it would appear to be better to use the Lax-Wendroff scheme with FCT. These two issues are significant if these schemes are to become of practical use. However, this paper will only present the underlying idea, acknowledging that achieving third order accuracy on uniform grids with different connectivities and an alternative method of enforcing positivity are necessary areas of future research.

The second test case involves the circular advection of the 'cone' given by the initial conditions

$$u \;=\; \begin{cases} \cos^2(2\pi r) & \text{for } \; r \leq 0.25 \\ 0 & \text{otherwise} \end{cases} \tag{33}$$

where $r^2 = (x + 0.5)^2 + y^2$, with velocity $\vec{\lambda} = (-2\pi y, 2\pi x)^{\mathrm{T}}$ around the domain $[-1, 1] \times [-1, 1]$, the solution being continually set to zero at each of the inflow

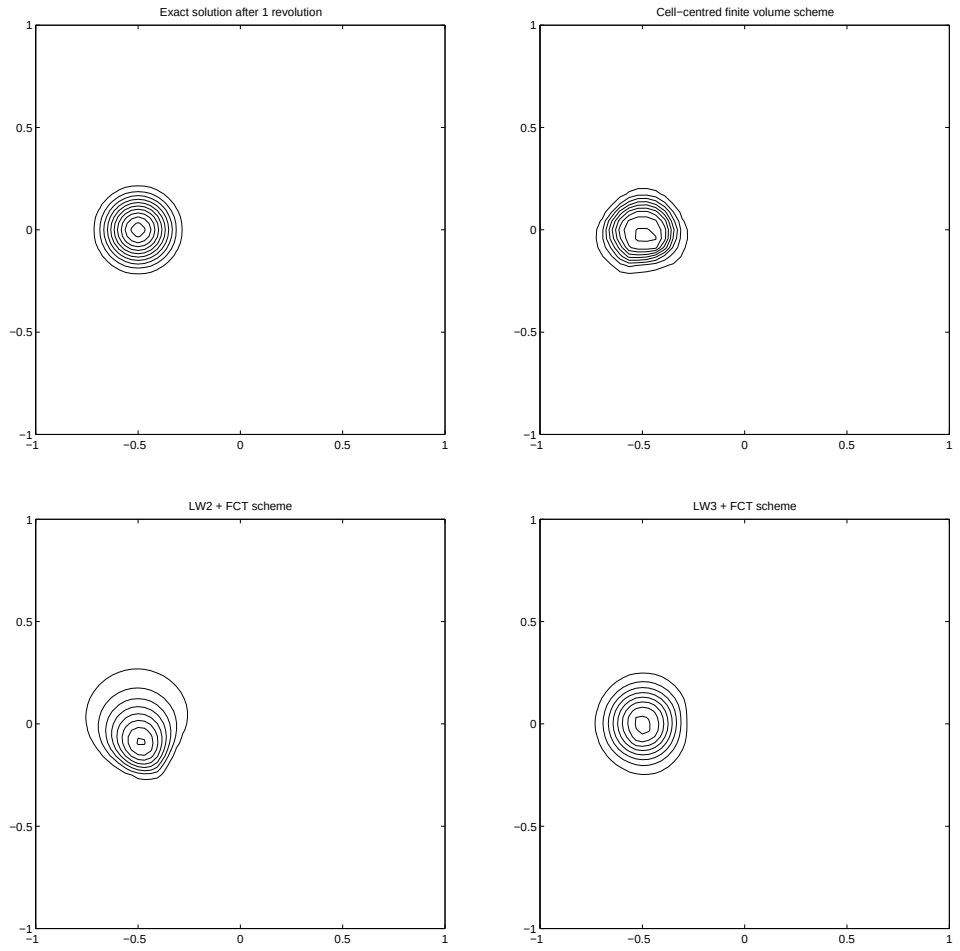

FIG. 8 Solutions after one revolution of the cosine-squared profile on a 64×64 type A grid (46×46 for the cell-centred scheme).

boundaries. The initial profile should be advected in a circle, around the centre of the domain, without change of shape until it returns to its original position when $t = 1.0$. In the numerical experiments the ratio $\Delta t/\Delta x = 0.08$, giving $|\nu_x| + |\nu_y| \leq 0.711$, with the maximum achieved at the corners of the domain.

The approximations obtained using the three higher order positive schemes from before on grids of type A are compared with the exact solution in Figure 8. Here the advantage of the third order scheme becomes clear. It removes the phase lag which occurs with the second order schemes and consequently preserves the shape of the profile much better, even though it doesn't significantly improve on the peak value, as indicated in Table 1. This gives an indication of why the error in the L_∞

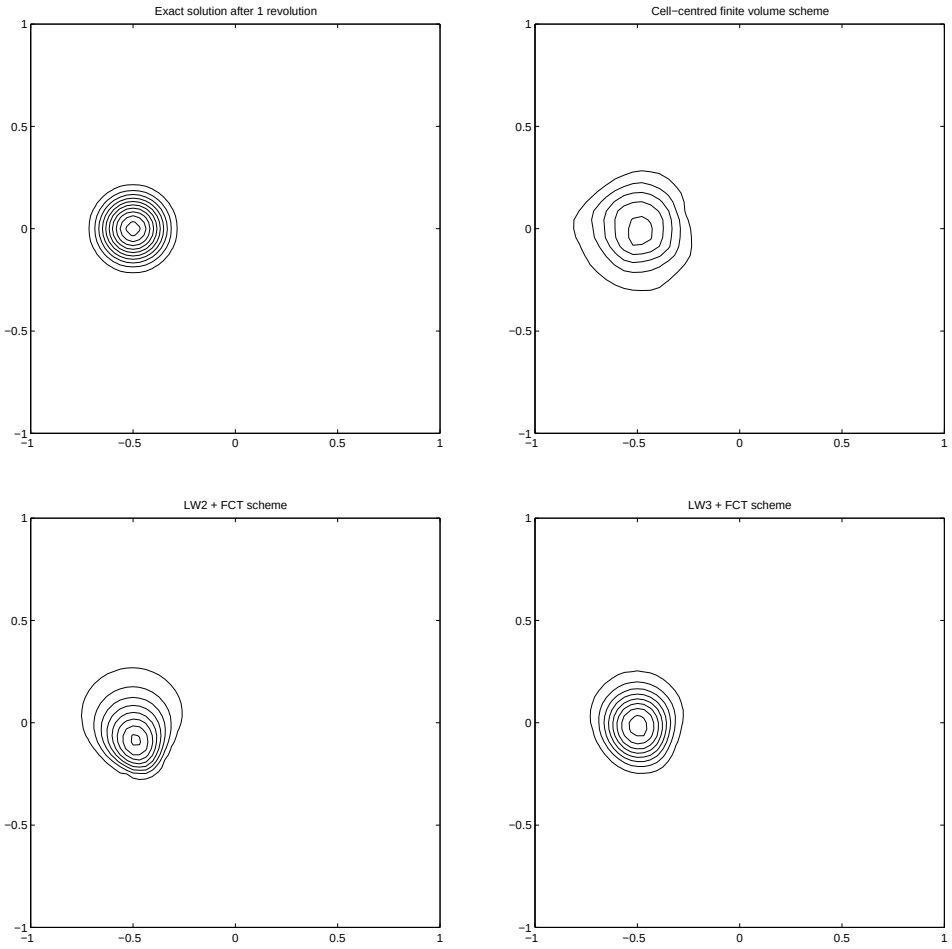

FIG. 9 Solutions after one revolution of the cosine-squared profile on a 64×64 type B grid (46×46 for the cell-centred scheme).

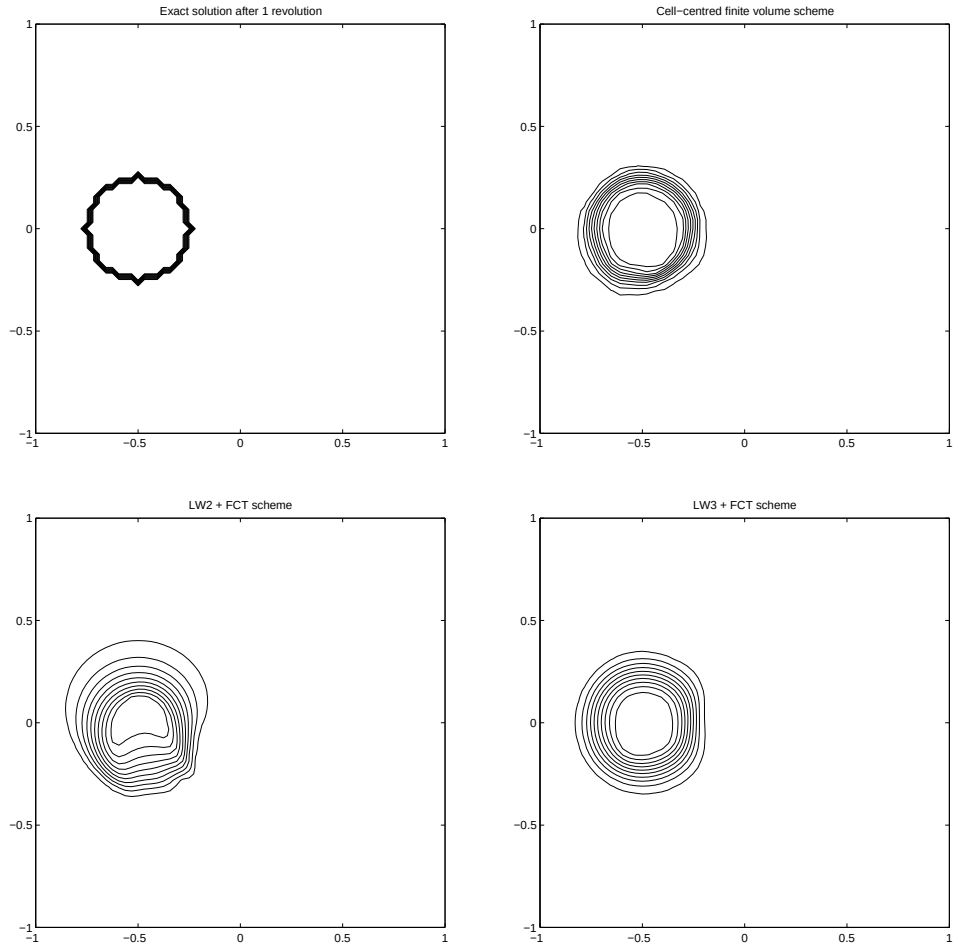

FIG. 10 Solutions after one revolution of the cylindrical profile on a 64×64 type A grid (46×46 for the cell-centred scheme).

norm isn't improved from the Lax-Wendroff scheme: fourth order accuracy would be required for this. Qualitatively, the results shown in Figure 9 (same test case, different grid) are very similar, but there is a notable deterioration in the quality of the cell-centred solution.

A similar effect is seen in results obtained using the same velocity profile but discontinuous initial conditions:

$$u = \begin{cases} 1 & \text{for } r \leq 0.25 \\ 0 & \text{otherwise} \end{cases} \tag{34}$$

with $r^2 = (x + 0.5)^2 + y^2$. The main difference to be seen in Figure 10 is the improvement in the results of the cell-centred scheme which is designed to be very good at maintaining steep gradients. Once more, changing to a type B grid has little effect on the qualitative nature of the results obtained using the cell vertex schemes.

5. CONCLUSIONS

A new fluctuation splitting approach has been presented for approximating the two-dimensional, *time-dependent* scalar advection equation on triangular grids. The method achieves third order accuracy in space and time by allowing the scheme to use a larger stencil. This can be done very efficiently within the framework of fluctuation splitting with little overhead beyond that of existing second order schemes. The initial results on uniform grids are promising.

There are still many aspects which require improvement. As mentioned in the text, an alternative to FCT should be sought for obtaining positivity: ideally through a mechanism incorporated within the scheme itself. Also, the current scheme is designed specifically for certain types of uniform grid and, although it can be used on arbitrary triangular grids, the additional accuracy is lost. Furthermore, the distribution does not depend continuously on the orientation of the advection velocity, which could cause problems in regions of flow which are close to equilibrium. It is likely that, rather than using Taylor series analysis, which is restricted to a uniform distribution of nodes, the coefficients in Eq. (22) should be derived from a local interpolant of the solution, or possibly by drawing an analogy with finite element methods which use quadratic test and trial functions – the mass-lumped schemes can be rewritten in the above framework of extended distribution

schemes. This would address the general accuracy and continuity issues, although an inherent positivity property may be more elusive. However, if these goals can be achieved then it should be simple to extend the scheme to nonlinear systems using any of the current methods applied to steady state problems.

ACKNOWLEDGEMENTS

The authors would like to thank Dr. P.K.Sweby of the University of Reading for his supervision of the early part of this work.

REFERENCES

[1] R.Abgrall, Toward the ultimate conservative scheme: Following the quest, *J. Comput. Phys.*, **167**(2):277–315, 2001.

[2] R.Abgrall and M.Mezine, Construction of second order accurate monotone and stable residual distributive schemes: the unsteady case, *J. Comput. Phys.*, **188**(1):16–55, 2003.

[3] R.Abgrall and P.L.Roe, High order fluctuation schemes on triangular meshes, *J. Sci. Comput.*, **19**:3–36, 2003.

[4] P.Batten, C.Lambert and D.M.Causon, 'Positively conservative high-resolution convection schemes for unstructured elements', *Int. J. Numer. Meth. Eng.*, **39**:1821–1838, 1996.

[5] P.Brufau, *Simulación bidimensional de flujos hidrodinámicos transitorios en geometrías irregulares*, Ph.D. thesis, Universidad de Zaragoza, 2000.

[6] D.Caraeni, M.Caraeni and L.Fuchs, A parallel multidimensional upwind algorithm for LES, AIAA paper 2001–2547, 15th AIAA CFD Conference, Anaheim, 2001.

[7] A.Csik and H.Deconinck, Space time residual distribution schemes for hyperbolic conservation laws on unstructured linear finite elements, in *Numerical Methods for Fluid Dynamics VII*, pp. 557–564, 2001.

[8] A.Csik, M.Ricchiuto, H.Deconinck and S.Poedts, Space-time residual distribution schemes for hyperbolic conservation laws, AIAA paper 2001–2617, 15th AIAA CFD Conference, Anaheim, 2001.

[9] H.Deconinck, K.Sermeus and R.Abgrall, Status of multidimensional upwind residual distribution schemes and applications in aeronautics, AIAA paper 2000–2328, 2000.

[10] H.Deconinck, R.Struijs, G.Bourgois and P.L.Roe, High resolution shock capturing cell vertex advection schemes for unstructured grids, *Computational Fluid Dynamics*, number 1994–05 in VKI Lecture Series, 1994.

[11] A.Ferrante, Solution of the unsteady Euler equations using residual distribution and flux corrected transport, VKI PR 1997–08, von Karman Institute for Fluid Dynamics, 1997.

[12] M.E.Hubbard and P.L.Roe, Compact high resolution algorithms for time dependent advection on unstructured grids, *Int. J. Numer. Meth. Fluids*, **33**(5):711–736, 2000.

[13] A.L.Laird, *A new method for solving the 2d advection equation*, M.Sc. dissertation, The University of Reading, 2000.

[14] R.Löhner, K.Morgan, M.Vahdati, J.P.Boris and D.L.Book, 'FEM-FCT: combining unstructured grids with high resolution', *Communications in Applied Numerical Methods*, **4**:717–729, 1988.

[15] J.März, 'Improving time accuracy for residual distribution schemes', VKI PR 1996–17, von Karman Institute for Fluid Dynamics, 1996.

[16] H.Paillère, H.Deconinck and E.van der Weide, Upwind residual distribution methods for compressible flow: an alternative to finite volume and finite element methods, in VKI LS 1997–02, von Karman Institute for Fluid Dynamics, 1997.

[17] M.Ricchiuto, Time accurate solution of hyperbolic partial differential equations using FCT and residual distribution, VKI SR 1999–33, von Karman Institute for Fluid Dynamics, 1999.

[18] C.-W.Shu and S.Osher, Efficient implementation of essentially non-oscillatory shock-capturing schemes, *J. Comput. Phys.*, **77**:439–471, 1988.

[19] D.Sidilkover and P.L.Roe, 'Unification of some advection schemes in two dimensions', ICASE Report 95-10, 1995.

[20] R.Struijs, 'A multi-dimensional upwind discretization method for the Euler equations on unstructured grids', Ph.D. Thesis, The University of Delft, The Netherlands, 1994.

[21] S.T.Zalesak, 'Fully multidimensional flux-corrected transport algorithms for fluids', *J. Comput. Phys.*, **31**:335–362, 1979.